THE JOURNAL OF PHYSICAL CHEMISTRY C

Article

pubs.acs.org/JPCC

Nucleation and Growth Mechanisms in Cu−Co Films

M. del C. Aguirre,*[,†,‡] H. Núñez Coavas,[‡] L. M. Fabietti,[†,‡] and S. E. Urreta[‡]

[†]Instituto de Física Enrique Gaviola de Córdoba, CONICET-UNC, 5000 Córdoba, Argentina

[‡]Facultad de Matemática, Astronomía y Física, FAMAF-UNC, Medina Allende s/n, Ciudad Universitaria, 5000 Córdoba, Argentina

Supporting Information

ABSTRACT: Nucleation and growth mechanisms in Co, Cu, and Co_xCu_{100-x} single films, and in Co_xCu_{100-x}/Cu bilayers, electrodeposited on $Cu_{70}Zn_{30}$ brass substrates, are studied by the constant potential technique. The recorded current−time transients (CTTs) are rather complex, and they extend for long times. Co, Cu, and Co_xCu_{100-x} alloys electrocrystallize onto brass, undergoing a process with more than a single maximum during the CTTs, as if two or more consecutive nucleation steps were present. The first stage of electrocrystallization in Co and Co_xCu_{100-x} films involves 3D instantaneous nucleation, but then, at long times, a progressive nucleation regime predominates. CTTs in Cu/brass and in Cu/Co_xCu_{100-x}/brass bilayers are well fitted by a 2DP progressive nucleation process at the initial stage, while for longer growing times a transition to a 3DP regime is observed, in which film growth becomes controlled by adatoms incorporation to the lattice. Film morphologies observed by SEM are consistent with these growth mechanisms. XRD results indicate that pure Co layers are *hcp* phase, while Cu and Cu−Co layers have an *fcc* lattice. Films are soft ferromagnetic, with an "in-plane" magnetization easy axis; there is evidence of crystallographic texture, which should be responsible for the higher coercivity observed in the "out-of-plane" configuration, with the applied field perpendicular to the film plane.

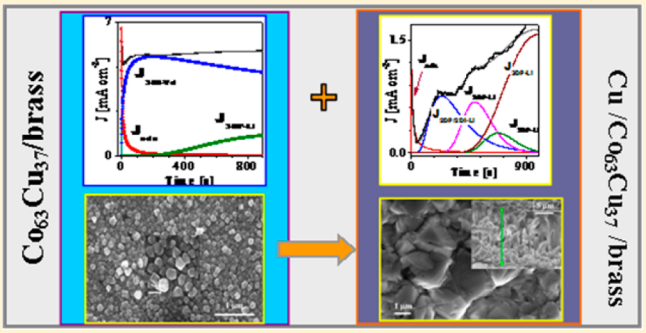

1. INTRODUCTION

Magnetic multilayers built up as stacks of alternating magnetic and nonmagnetic layers are important designs in magnetic sensor technologies and magnetoelectronics. These magnetic films and multilayer systems are usually prepared by techniques such as plasma deposition, sputtering, and chemical or physical vapor deposition.[1] In the special case of Co/Cu films/multilayers, the most widely used process is electrodeposition,[2,3] with Cu and Co electrodeposition onto foreign substrates being a matter of great importance, particularly in thick films technologies for microelectronics.

To achieve a better control of structural, magnetic, and/or electronic properties of these multilayer devices, it is necessary to describe in detail the mechanisms controlling electrodeposition, their kinetics, and the interfacial phenomena affecting crystallization. Cyclic voltammetry and chronoamperometry are electrochemical experimental techniques well suited for these purposes. Potentiostatic current−time transient curves (CTTs) are usually interpreted on the basis of theoretical models[2,4] describing nucleation and early nucleus growth regimes; from these data, it is possible to determine whether nucleation is instantaneous (I) or progressive (P), with 2D or 3D growth geometry, and also if this initial growth is controlled by ion volume diffusion (Vd) or by adatoms incorporation/detachment at the lattice interface (Li); from the experimental current data, kinetic parameters closely related to the crystallization process may be estimated.

Fundamental studies of nucleation mechanisms of copper and cobalt onto different substrates have been reported;[3,5−9] it is found that the number of nuclei formed on the surface strongly depends on the overpotential, which determines the deposit granularity, affecting the final magnetic and/or electronic properties.[3]

In the case of Cu−Co films, the CTTs are not always simple, with more than a single maximum observed during the process, as illustrated in section 4. More than a single maximum within the transients indicates that cobalt and/or copper electrocrystallization takes place in two or more consecutive nucleation steps. Multiple maxima in a transient have been attributed to three different mechanisms.[5,8−11] The first one, proposed by Abyaneh et al.,[6,10] is related to a process of death and rebirth of nucleation centers; the second one suggests the existence of different macroscopic zones on the electrode surface,[10] and a third one is related to nucleation of different chemical species.

To properly identify and interpret each step during the deposition process, many authors[5,11−13] separately treat each range of the total transient current curve by using existing mathematical formalisms.[4,14−20] Despite the multistage character of the current transient, these authors analyze the current curve following the same protocol as for single peak profiles.

Received: May 17, 2016
Revised: August 30, 2016
Published: September 2, 2016

DOI: 10.1021/acs.jpcc.6b04994
J. Phys. Chem. C 2016, 120, 22142−22154

The local maxima in the $J(t)$ curve are associated with sequential nucleation steps, and the total curve is normalized relative to each pair of parameters $(J_{m,i};\ t_{m,i})$ at a time, to compare the data associated with each maximum with the curve predicted by Scharifker–Hills (SH)[14] and Bewick, Fleischmann, and Thirsk (BFT)[15] models. In the first case, a growth mechanism controlled by ion diffusion (Vd) is considered, while for the second one, adatom incorporation/release processes at the lattice interface (Li) are proposed to be the rate-controlling process.

Palomar Pardavé et al.[8] also reported a detailed characterization of potentiostatic current transients associated with 2D to 2D and 2D to 3D nucleation regime transitions during silver deposition; depending on the applied deposition potential, different pathways may be identified during a single potentiostatic current curve. Similar phenomena have been reported in cobalt nucleation onto glassy carbon.[5] The mechanisms of cobalt and copper nucleation onto substrates like glassy carbon and both poly- and single-crystalline Cu have already been explored.[5,6,8,11,13] However, the kinetics of electrocrystallization of copper and cobalt onto brass substrates is still unknown.

In this Article, we report our results related to the mechanisms of electrocrystallization in Co, Cu, and Co_xCu_{100-x} alloy films, and in Co_xCu_{100-x}/Cu double layer films, all deposited on Cu-30 wt % Zn brass substrates. On the contrary to the conventional approach, normally focused on nucleation–growth process at very short deposition times, we consider processes leading to current–time transient extended in time. We investigate the deposition process by measuring the current profiles for relatively large times (10–30 min). The multistep current–time profiles obtained are analyzed assuming that steps contributing to the global current curve may be described by the simple superposition of successive peak contributions, associated with distinct stages in the process. Each peak is then compared to the corresponding dimensionless curves provided by different single-ion models for the early crystallization stages, even in the case of simultaneous deposition of Cu and Co ions. From this analysis, effective values for deposition parameters are obtained.

These deposition mechanisms/processes are then correlated with the surface film morphology, the microstructure, and their magnetic hysteresis properties.

2. METHODOLOGY

2.1. Experimental Procedures. All chemical reagents used were of analytical grade: $CuSO_4{\cdot}5H_2O$ (Sigma-Aldrich), $CoSO_4{\cdot}7H_2O$ (Sigma-Aldrich), and H_3BO_3 (Cicarelli). Brass ($Cu_{70}Zn_{30}$) foils, 0.3 mm thick (Alfa Aesar), were used as substrates; before the metal electrodeposition, they were mechanically polished up to 1 μm diamond paste.

Electrochemical deposition of Co, Cu, or Co–Cu layers was made in a potentiostat/galvanostat Autolab 302N, under inert atmosphere. The reference electrode was Ag/AgCl (3 M KCl), the working electrode was the polished brass foil, while Pt was used as the counter electrode. Cobalt was deposited from 0.1 M $CoSO_4$ /H_2SO_4 and 0.1 M H_3BO_3 solution of pH 3, at −0.8 V for 30 min. Copper electrodeposits were built up from 0.1 M $CuSO_4$/H_2SO_4 and 0.1 M H_3BO_3 of pH 3, at −0.8 V for 15 min. A nominal $Co_{95}Cu_5$ alloy was fabricated from 0.1 M $CoSO_4$ and 0.00526 $CuSO_4$ solutions in 0.1 M H_3BO_3 at pH 3, using a constant potential (CP) of −0.8 V during 15 min. To obtain bilayers, samples of $Co_{95}Cu_5$ processed at −0.8 V for 12 min were used as substrates for electrodepositing Cu at −0.8 V for 15 min.

Boron content in the films was measured in a microprobe JEOL JXA 8230, with a LDEz Kα crystal (188.53 mm) and a current of 50 nA. No traces of boron could be detected in the films with this technique. Smaller traces (1.9 ± 0.1) ppm were further explored in the films by the ICP-MS (inductively coupled plasma mass spectrometry) method in an AGILENT 7500cx device (low detection limit = 0.539 ppm; low quantification limit = 1.851 ppm).

Co electrodeposition onto brass was evaluated by cyclic voltammetry (CV), between −0.17 and −0.8 V, and between −0.3 and −1.05 V at a scan rate of 10 mV/s. All of these procedures were carried out at room temperature, under a nitrogen atmosphere.

No contribution of the less noble component of the substrate (Zn from brass during Cu deposition, or Co from the Cu–Co alloy during the bilayer Cu deposition) to the current response during deposition could be detected (see the Supporting Information).

The resulting structures were characterized by X-ray diffraction (XRD) measured in a Philips PW3830 diffractometer using Cu Kα radiation (λ = 1.5418 Å), in the 2θ range from 30° to 95° in Bragg–Brentano configuration. Film morphology and composition were analyzed in a scanning electron microscope (FE-SEM) Zeiss. The room-temperature hysteresis loops were measured in a vibrating sample magnetometer (VSM) Lakeshore 7300, with a maximum field up to 1.5 T; the external field was applied parallel (PA) and perpendicular (PE) to the substrate plane.

2.2. Nucleation and Growth Kinetic Models. Electrocrystallization of metals takes place at an electronic conducting substrate/ionic conducting electrolyte interface following, in general, three stages: (1) formation of metal adatoms, onto native or foreign substrates via adsorption, (2) two-dimensional (2D) and three-dimensional (3D) metal phase formation by nucleation and cluster growth, and (3) crystal growth of the 3D metal bulk phase.

Monitoring with chronoamperometric techniques the current versus time curves during metal deposition from the feed solution allows one to obtain a family of current time transients (CTTs) arising from the process. The shape of these CTTs is sometimes complex and largely depends on the applied potential.

As previously mentioned, different mechanisms for crystallite nucleation and growth have been proposed to describe the CTT curves for single pure elements: one is the well-known theoretical model proposed by Scharifker–Hills (SH model)[14] for instantaneous (I) or progressive (P) nucleation of three-dimensional (3D) hemispherical nucleus, with growth rate controlled by ion volume diffusion (Vd); another one is the traditional model proposed by A. Bewick, M. Fleischman, and H. R. Thirsk (BFT model)[15] for a two-dimensional (2D, I or P) nucleation mechanism, with crystallite growth further controlled by the incorporation of atoms into the lattice interface (Li).

These models have also been successfully applied to describe electrodeposition of two different elements to obtain alloyed Fe–Co thick films;[22] in this case, the values of the parameters estimated from the CTT curves are in fact effective values, depending on the two species involved in the deposition process.

DOI: 10.1021/acs.jpcc.6b04994
J. Phys. Chem. C 2016, 120, 22142–22154

3D type nucleation processes, in which nuclei growth is controlled by adatoms incorporation to the lattice (Li), have been proposed by Armstrong−Fleischmann and Thirsk (AFT).[17] This model describes a three-dimensional (3D) instantaneous or progressive nucleation mechanism, with nucleus growth limited by incorporation of atoms at lattice sites on the surface of the solid (Li); it takes into account the overlapping of growing nuclei with the geometry of right-circular cones.

Experimental and theoretical current transients[6,10,17] corresponding to all of these mechanisms exhibit a maximum, from which dimensionless curves may be constructed, eqs 1−6. In fact, the predictions of these models are frequently displayed in a dimensionless J/J_m versus t/t_m curve, with J_m the maximum current value and t_m the time at which this maximum current is achieved. These single peak model curves are plotted together with the normalized experimental data, and the controlling mechanism is determined by simple comparison.

The dimensionless theoretical curves, corresponding to those mechanisms or regimes[14,15,17] most frequently identified during early stages of electrodeposition, have been derived to be as follows (see Appendix):

$$\frac{j}{j_m} = \left(\frac{1.9542 t_m}{t}\right)^{1/2}\left\{1 - \exp\left[1.2564\left(\frac{t}{t_m}\right)\right]\right\} \quad \text{3DI-Vd} \tag{1}$$

$$\frac{j}{j_m} = \left(\frac{1.2254 t_m}{t}\right)^{1/2}\left\{1 - \exp\left[2.3367\left(\frac{t}{t_m}\right)^2\right]\right\} \quad \text{3DP-Vd} \tag{2}$$

$$\frac{j}{j_m} = \left(\frac{t}{t_m}\right)\left\{\exp\left[\left(\frac{t^2 - t_m^2}{2t_m^2}\right)\right]\right\} \quad \text{2DI-Li} \tag{3}$$

$$\frac{j}{j_m} = \left(\frac{t}{t_m}\right)^2\left\{\exp\left[\left(\frac{-2(t^3 - t_m^3)}{3t_m^3}\right)\right]\right\} \quad \text{2DP-Li} \tag{4}$$

$$\frac{j}{j_m} = 4\left\{1 - \exp\left[-\frac{0.6913 t^2}{t_m^2}\right]\right\}\exp\left(-\frac{1.386 t^2}{t_m^2}\right) \quad \text{3DI-Li} \tag{5}$$

$$\frac{j}{j_m} = 4\left\{1 - \exp\left[-\frac{0.6913 t^3}{t_m^3}\right]\right\}\exp\left(-\frac{1.386 t^3}{t_m^3}\right) \quad \text{3DP-Li} \tag{6}$$

Once the operative mechanism is identified, different structural and kinetic parameters may be estimated as illustrated in the Appendix. As eqs 1−6 have been derived considering single-ion processes, the parameter values obtained after fitting our experimental Cu−Co data should be, in all of these cases, taken as effective values, representing the more complex process involving the simultaneous electrodeposition of two different species.

3. RESULTS AND DISCUSSION

3.1. Electrocrystallization Process. *Co/Brass.* The cyclic voltammogram obtained during Co deposition from a 0.1 M Co^{2+} solution onto a $Cu_{70}Zn_{30}$ (brass) substrate, measured at a scan rate of 10 mV s^{-1}, is shown in Figure 1. In aqueous

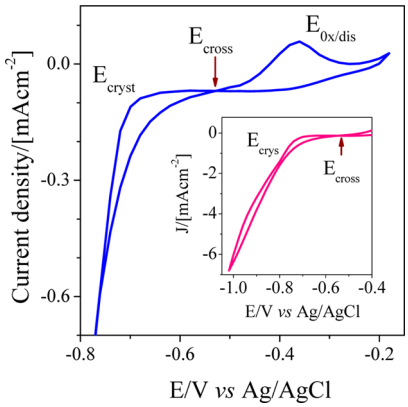

Figure 1. CV curve obtained during Co deposition from $CoSO_4$ 0.1 M/H_2SO_4 pH 2, onto a brass substrate at 10 mV/s.

solutions, cobalt is present in the form of a $Co(H_2O)_6^{2+}$ aqueous complex.[20] The equilibrium redox potential of $Co(H_2O)_6^{2+}/Co$ calculated by the Nernst equation is $E^0_{NHE} = -0.306$ V, and $E^0_{Ag/AgCl} = -0.526$ V. During the forward scan toward the negative potentials, the onset of Co deposition was at about −0.68 V (E_{crys}) vs Ag/AgCl, and the cathodic current, corresponding to the increase in the density of nuclei and crystal growth, sharply increased. Upon the swept reversal, the overcrossing potential (E_{cross}) was at −0.529 vs Ag/AgCl, which is typical of the formation of a new phase involving a nucleation process. Sometimes, when E_{cross} is independent of the switching potential, the crossover potential (−0.529 V) may be associated with the thermodynamic potential of M^{n+}/M. This is possible because the deposition overpotential of metal ions is lower when the crystallographic misfit between the substrate and the deposited metal is negligible. The further scanning toward positive potentials resulted in an anodic peak, which corresponded to the oxidation/dissolution of the cobalt deposits. Here, it was possible to observe a principal peak at around −0.36 V vs Ag/AgC, preceded by an almost negligible shoulder (at −0.377 V vs Ag/AgCl). This shoulder is likely to arise from the dissolution of a hydrogen-rich cobalt phase. The inset in Figure 1 illustrates the large hydrogen evolution taking place in the cathode direction at higher negative potentials.

In this sense, boric acid is added to the electrolyte to control local pH, which may increase due to proton reduction, leading to a parallel hydrogen evolution reaction (HER). Controlling OH^- generation, the formation of hydroxilated Co species[21] diminishes. This guarantees the major quantity of free Co^{2+} ions species in the solution, eliminating hydroxides incorporation into the deposit. In this work, the shape of the CV reduction wave up to −0.8 V vs Ag/AgCl does not show any evidence of boric acid reduction with protons nor of its incorporation into the film.

As previously indicated, no traces of boron were detected in these films, previously exfoliated from the substrate, with the microprobe. Smaller concentrations then were further explored by the ICP-MS method. The bilayer film, with the highest exposition time to H_3BO_3 0.1 M, was found to contain only (1.9 ± 0.1) ppm of boron, a quite low value, very close to the low quantification limit of the method (1.851 ppm).

Chronoamperometry. A family of current−time transients, corresponding to Co deposition from 0.1 M $CoSO_4$ onto brass at −0.9, −0.85, and −0.8 V, for 30 min is built up. The CTTs profiles are complex and depend on the applied potential; they clearly exhibit more than a single maximum, indicating that

DOI: 10.1021/acs.jpcc.6b04994
J. Phys. Chem. C 2016, 120, 22142−22154

cobalt electrocrystallization involves two or more successive nucleation steps. The CTTs also show that the nucleation rate increases, and the mechanism becomes more complex when larger potentials are imposed. A possible explanation for multi steps considers that Co is present in the solution in two possible oxidation states, as Co(II) and Co(III), and a charge transfer Co(III) → Co(II) may happen[8] prior to electrodeposition. However, this step would not appear under our experimental conditions, because it occurs at potential values more positive than those analyzed here.

The total current curve corresponding to Co electrodeposition onto brass at −0.8 V/30 min is shown in Figure 2a together with the four peak functions contributing to the

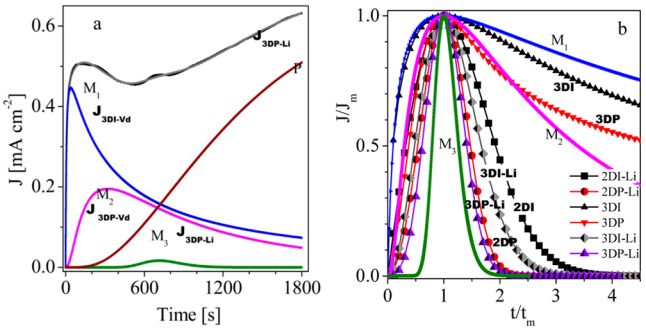

Figure 2. (a) CTT for Co deposition showing the different contributions. (b) Dimensionless curves J/J_m vs t/t_m.

total profile, indicating consecutive nucleation steps. The analysis of the CTT curve is performed by considering that it results from the superposition of as many peak functions (Lognormal profiles) as local maxima are detected, each one representing one process step. The normalized profile of each one of these peak contributions is then compared to the different model curves in eqs 1−6 to identify which is the rate-controlling mechanism.

The total current density transient, $J(t)$, for Co electrodeposition onto brass is then described by

$$J(t)_{Co} = J_{3DI\text{-}Vd}(t) + J_{3DP\text{-}Vd}(t) + J_{3DP\text{-}Li}(t) + J_{3DP\text{-}Li}(t) \quad (7)$$

where each J_k contribution corresponds to a local maximum. It may be observed that the first current maximum (M_1) closely follows the response predicted for 3DI instantaneous nucleation, Figure 2b. Assuming that the growth is controlled by volume diffusion (Vd) (the Scharifker−Hills model), parameters such as the effective diffusion coefficient (D_0) and the nucleus density number N_0 at steady state may be estimated, as shown in eqs A2 and A3, in the Appendix. The resulting values are listed in Table 1.

The subsequent step in the process (M_2) is associated with a 3D-Vd progressive nucleation regime, but the onset of a 2D-Li or 3D-Li nucleation process, limited by the incorporation (disincorporation) of atoms to the growing (dissolving) nuclei, cannot be excluded. Although the actual nucleation mechanisms are difficult to describe in detail, it is known that the difference between 2DP and 3DP nucleation is the absence of damped oscillations in the latter case.[2,4] It is worth noting that the process leading to M_2 largely overlaps with the others. Finally, 3DP-Li (lattice incorporation) processes lead to the small M_3 maximum and also to the curve P. The appearance of a 3D-Li regime involves an important contribution to the whole density current arising in a higher value of the perpendicular incorporation constant rate (k_2), from 0.33 × 10^{-9} to 10.55 × 10^{-9} mol s^{-1} cm^{-2}. In this way, a growth mechanism controlled by lattice incorporation enhances texture development. This growth mechanism is reflected by the columnar morphology observed in SEM micrographs (lateral view in Figure 9a). In addition, at lower pH, cobalt electrodeposition may be accompanied by hydrogen evolution,[16] promoting hydrogen codeposition. This leads to mixing in the solution and introduces changes in the mass transfer limitations at the electrode surface. Thus, the hydrogen evolution influences the cobalt crystal nucleation and growth kinetic; it is the most effective way to reduce mass transport limitations for electrochemical processes in mixed activation−diffusion-controlled regimes.

It has been reported[8,23] that cobalt reduction on glassy carbon follows a three-dimensional instantaneous nucleation mechanism, resulting in cobalt films with typical nodular structure. A 3DI-Vd mechanism is also found in the present work for short times (30 s), but other 3DP contributions become dominant at longer times. However, for cobalt deposition on a copper foil substrate from 0.1 M $CoCl_2$, without any addition of boric acid, we found that Co deposition on Cu substrates is well described by a 3DP-Vd mechanism,[22] while for Co on brass studied in the present work, an initial 3DI regime is observed with a transition to a 3DP one, controlled by diffusion, in the second stage.

$Co_{63}Cu_{37}$/Brass. The electrocrystallization of Co_xCu_{10-x} onto ($Cu_{70}Zn_{30}$) brass, from a cobalt sulfate electrolyte with the addition of a small amount of copper ions (in a mol ratio Co:Cu (95:5)), was performed at −0.8 V for 10, 12, 15, and 30 min. Three different deposits were performed for 12 min to

Table 1. Scharifker−Hills[14] and AFT[17] Model Parameters for Co/Brass

	Co, −0.8 V, 30 min	M_1	M_2	M_3	P
	t_m [s]	40	323	712	1779
	$10^{-4}J_m$ [A cm^{-2}]	4.46	1.96	0.17	5.09
$J_{3DI\text{-}Vd}$	K	0.13			
	D_0 [10^{-7} cm^2 s^{-1}]	1.31			
	10^5N_0 [cm^{-2}]	5.85			
$J_{3DP\text{-}Vd}$	k'		0.17		
	D_0 [10^{-7} cm^2 s^{-1}]		1.28		
	AN_∞ [10^2 s^{-1} cm^{-2}]		6.55		
	10^5N_s [cm^{-2}]		1.23		
$J_{3DP\text{-}Li}$	k_2 [10^{-9} mol s^{-1} cm^{-2}]			0.35	10.55
	$AN_0k_1^2$ [10^{-11} mol^2 cm^{-6} s^{-3}]			4.18	0.268

DOI: 10.1021/acs.jpcc.6b04994
J. Phys. Chem. C 2016, 120, 22142−22154

evaluate reproducibility. All of the measured transient current versus time curves are displayed in Figure 3a. The composi-

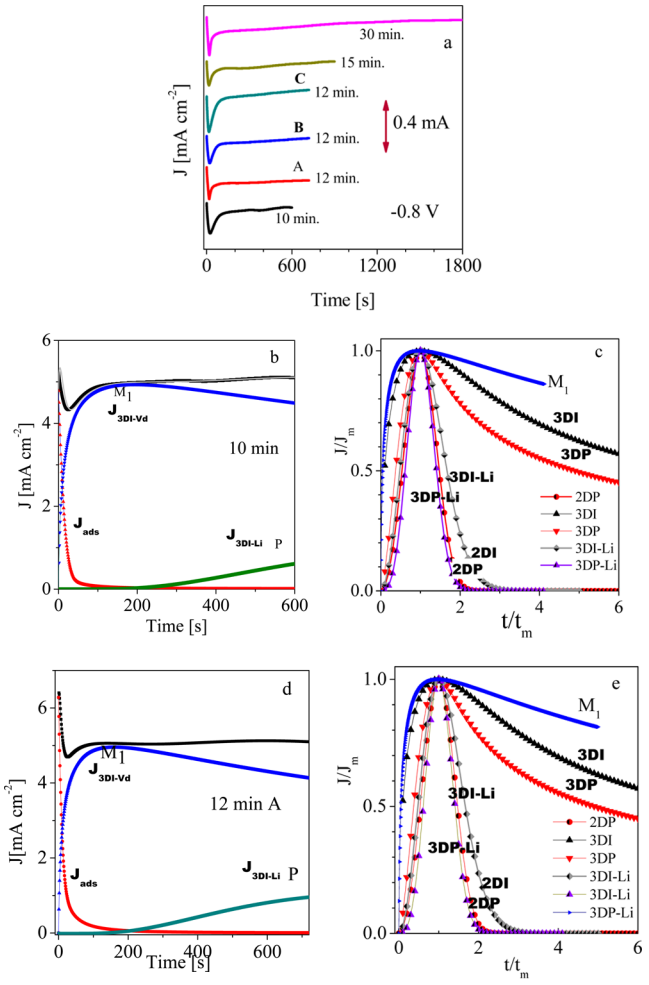

Figure 3. (a) CTT of Co:Cu (95:5) mol ratio feed, deposited onto brass at −0.8 V, for different times: (b) 10 min, (c) curves J/J_m vs t/t_m corresponding to $Co_{63}Cu_{37}$/ brass in (b); (d) 12 min, and (e) dimensionless curve from (d).

tional analysis of the alloy films synthesized resulted as $Co_{63\pm2}Cu_{37\pm2}$. The analysis of the current−time transients suggests that crystallization mainly proceeds by three-dimensional growth, with a predominant instantaneous nucleation regime. In the presence of copper ions, an important contribution to the global current density is observed at the beginning, arising from a Langmuir-type adsorption−desorption process of ions(II), involving the double layer charge;[18] Figure 3b,c shows the CTT and the dimensionless t/t_m versus J/J_m curves for $Co_{63}Cu_{37}$ after 10 min deposition, respectively, and Figure 3d,e after 12 min deposition. Both CTT curves exhibit an important and wide initial maximum (M_1) at an average time of ∼177 s, attributed to instantaneous nucleation and tridimensional growth, controlled by volume diffusion (Scharifker−Hill model). This kinetics was also observed by Min Gu et al.[24] in the electrocrystallization of cobalt−copper alloys on glass carbon electrodes, from Co-rich sulfate solutions. They find that during the first 30 s deposition mainly proceeds by a 3DI-Vd mechanism, as is found in the stage (M_1) in the present work. Curves P in both samples keep a 3D instantaneous nucleation regime, but with growth controlled by adatoms incorporation into the lattice (Li). Assays with longer deposition times were carried out. Samples deposited during 15 min at −0.8 V showed similar features, with a first maximum (M_1) at 177 s concordant with a diffusional kinetic of 3DI nucleus and the curve P with a 3DI nucleation and charge transfer control (Li) (see Figure 4a,b). Curves P, in CTTs of Figures 3b,d and 4a, involve a growth regime not limited by diffusional current, but by the activation across the interface or a mixed one. Curves P were analyzed by comparison with the dimensionless curves J/J_m versus t/t_m [given in the Appendix] and also by determining the relationship between $J(t)$ and t^n at short times of the 3D-Li current transient. In fact, at short times, the arguments of the exponential terms are sufficiently small, and current becomes (see Appendix):

$$J(t) \cong \frac{zFk_2\pi M^2 k_1^{\,2} N_0}{\rho^2} t^2 \quad \text{3DI} \tag{8}$$

and

$$J(t) \cong \frac{zFk_2\pi M^2 A k_1^{\,2} N_0}{3\rho^2} t^3 \quad \text{3DP} \tag{9}$$

It is then possible to evaluate J versus t^2 and J versus t^3 curves in Figures 3b,d and 4b, for the initial times of P curves. The linear regression performed in each case demonstrated a much better correlation factor for the curve j versus t^2 ($r^2 = 0.990 \pm 0.004$), in agreement with a 3D instantaneous nucleation mechanism, than for progressive j versus t^3 ($r^2 = 0.97 \pm 0.01$) mechanism. A

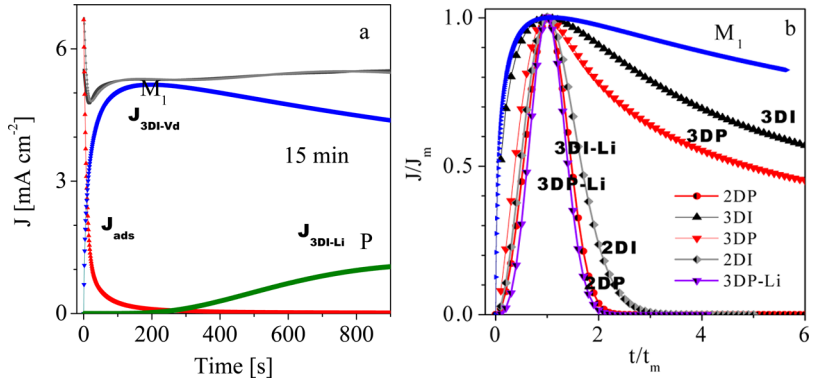

Figure 4. (a) CTT of $Co_{63}Cu_{37}$, deposited at −0.8 V for 15 min, onto brass. (b) Dimensionless curves J/J_m vs t/t_m corresponding to $Co_{63}Cu_{37}$/brass in (a).

DOI: 10.1021/acs.jpcc.6b04994
J. Phys. Chem. C 2016, 120, 22142−22154

3DI mechanism is then proposed and further verified by the dimensionless curve fit.

The total current density transient, $J(t)$, for the $Co_{63}Cu_{37}$ film (at 10, 12, and 15 min) may be then expressed as

$$J(t)_{Co_{63}Cu_{37}} = J_{ad}(t) + J_{3DI\text{-}Vd}(t) + J_{3DI\text{-}Li}(t) \quad (10)$$

Samples deposited during 30 min (Figure 5a,b) revealed that besides the main maximum (M_1) with a 3DI diffusion-

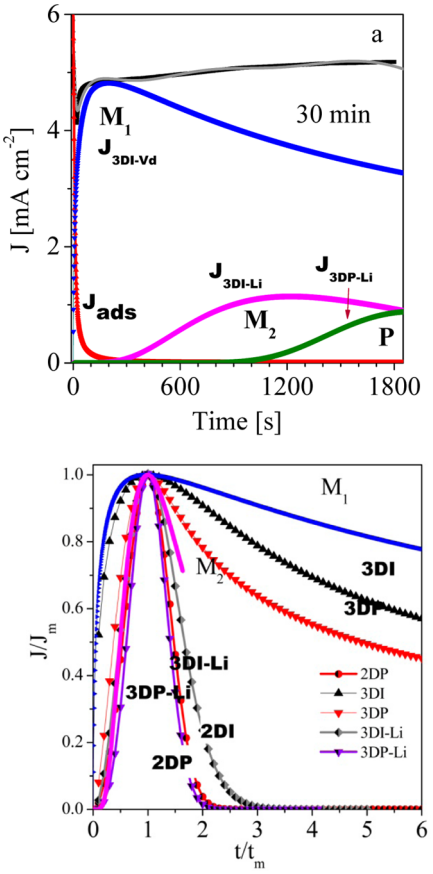

Figure 5. (a) CTT of $Co_{63}Cu_{37}$, deposited at −0.8 V for 30 min, onto brass. (b) Dimensionless curves J/J_m vs t/t_m corresponding to $Co_{63}Cu_{37}$/brass in (a).

controlled mechanism, a second maximum (M_2) appears at 1221 s, consistent with mechanisms 3DI-Li ($t/t_m < 1$) or 2DI-Li ($t/t_m > 1$) according to the dimensionless curves. In agreement with the mechanisms proposed for lower deposition times, the curve M_2 is considered as the continuation of curve P presented at 10, 12, or 15 min, with a character 3DI-Li. Finally, curve P in the sample synthesized by 30 min (Figure 5a) is compared to a character instantaneous or progressive. The analysis at short times on the basis of the 3D-Li model indicated that linear regressions of j versus t^2 and of j versus t^3 of curve P in the sample synthesized by 30 min were quite close, with a factor $r^2 = 0.990 \pm 0.003$. Thus, in this last stage, the mechanism is transitional, from instantaneous to progressive turning to a 3DP-Li regime. The total current density transient, $J(t)$, for the $Co_{63}Cu_{37}$ film (at 30 min) may be then expressed as

$$J(t)_{Co_{63}Cu_{37}} = J_{ad}(t) + J_{3DI\text{-}Vd}(t) + J_{3DI\text{-}Li}(t) + J_{3DP\text{-}Li}(t) \quad (11)$$

On the basis of the Langmuir-type adsorption−desorption equilibrium and the time dependence of this current component, a quantitative estimate of the ions (II) adsorption contribution is given by[18] $J_{ad}(t) = k_{ads}\exp(-k_{des}t)$, where $k_{ads} = k_{des}q_{ads}$. In the Appendix, detailed expressions for current densities $J_{3DI\text{-}Vd}$ (eqs A1−A3), $J_{3DI\text{-}Li}$ (eqs A17−A20), and $J_{3DP\text{-}Li}$ (eqs A21−A24) are given. The parameter values estimated are listed in Table 2 (10 min), Table 3 (12 min), Table 4 (15 min), and Table 5 (30 min).

Table 2. S−H[14] and AFT[17] Theory Parameters for $Co_{63}Cu_{37}$/Brass, 10 min, and Kinetic Parameters of Langmuir Adsorption for the Electrochemical Double Layer (DL) Charge[18]

	Co−Cu, −0.8 V, 10 min	M_1	P	DL
	t_m [s]	194	595	
	J_m [10^{-3} A cm^{-2}]	1.284	0.21	
$J_{3DI\text{-}Vd}$	D_0 [10^{-6} cm^2 s^{-1}]	5.27		
	N_0 [10^3 cm^{-2}]	3.11		
$J_{3DI\text{-}Li}$	k_2 [10^{-9} mol cm^{-2} s^{-1}]		4.35	
	$k_1^2N_0$ [10^{-8} mol^2 s^{-2} cm^{-6}]		1.37	
J_{ads}	Q_{ads} [mC cm^{-2}]			17.1
	k_{ads} [mA cm^{-2}]			1.3
	k_{des} [s^{-1}]			0.075

Cu/Brass. Cu electrocrystallization from copper sulfate electrolyte onto ($Cu_{70}Zn_{30}$) brass substrate was performed at −0.8 V, for 15 min. The first contribution to the total current curve $J(t)$, displayed in Figure 6a, is a decreasing current, which may arise from the adsorption of copper atoms onto the surface, from the partial reduction of Cu(II) to Cu(I) as described in ref 19 and/or related to the double layer charge.[18] Both, adsorption or ion/electron transfer precedes the copper nuclei formation. Contributions M_1 (peak at 147 s) with a 2DP-Li regime and M_2 and M_3, both with 3DP-Li character, then are detected. Cu ions are discharged and directly incorporated into the lattice of supercritical copper crystals when they are formed on the electrode surface.[19] 3D progressive nucleation, controlled by interface transfer, predominates at longer times, after the 2D process, and this is consistent with the observed morphology. The presence of M_2 and M_3 (both 3DP-Li) exhibits different kinetic characteristics (see Table 6), because k_2 and $N_0Ak_1^2$ decrease as the electrodeposition time increases, and it is probably related to differences in the surface microstructure. The last step is a 3DI-Li contribution (M_4), followed by a 3DP-Li peak P, as illustrated in Figure 6a,b. The appearance of 3DI nuclei means that they are generated independently of the nuclei in 2DP-Li (M_1) as well as the subsequent steps (M_2 and M_3). It involves the start of a new regime, controlled by charge−transfer, which continues in the curve P. This is consistent with a decreasing growth constant k_2, from 9.89×10^{-9} mol cm^{-2} s^{-1} (3DI, curve M_4) to 6.1×10^{-9} mol cm^{-2} s^{-1} (3DP-Li, curve P).

Next, $J(t)$ may be expressed as

$$J(t)_{Cu} = J_{ads\text{-}DL}(t) + J_{2DP\text{-}Li}(t) + J_{3DP\text{-}Li}(t)(M_2, M_3) + J_{3DI\text{-}Li}(t) + J_{3DP\text{-}Li}(t) \quad (12)$$

The resulting parameter values are listed in Table 6.

A different behavior has been reported[7] for the nucleation mechanism of copper during electrodeposition on glassy carbon

DOI: 10.1021/acs.jpcc.6b04994
J. Phys. Chem. C 2016, 120, 22142−22154

Table 3. S−H and AFT Theory Parameters for $Co_{63}Cu_{37}$/Brass, 12 min, and Kinetic Parameters of Langmuir Adsorption for the Electrochemical Double Layer (DL) Charge[18]

		12 min A			12 min B			12 min C		
	Co−Cu, −0.8 V, 12 min	M_1	P	DL	M_1	P	DL	M_1	P	DL
	t_m [s]	160	716		186	720		188	720	
	J_m [10^{-3} A cm^{-2}]	1.21	0.25		1.25	0.21		1.21	0.20	
$J_{3DI\text{-}Li}$	k_2 [10^{-9} mol cm^{-2} s^{-1}]		5.18			4.35			4.14	
	$N_0k_1^2$ [10^{-9} mol^2 cm^{-6} s^{-2}]		9.47			9.36			9.36	
$J_{3DI\text{-}Vd}$	K	0.13			0.13			0.13		
	D_0[10^{-6} cm^2 s^{-1}]	3.86			4.79			4.54		
	N_0 [10^3 cm^{-2}]	5.39			3.45			3.61		
J_{ads}	Q_{ads} [mC cm^{-2}]			18.5			12.9			10.9
	k_{ads} [mA cm^{-2}]			1.5			1.52			1.04
	k_{des} [s^{-1}]			0.082			0.12			0.09

Table 4. S−H[14] and AFT[17] Model Parameters for $Co_{63}Cu_{37}$, 15 min, and Kinetic Parameters of Langmuir Adsorption for the Electrochemical Double Layer (DL) Charge[18]

	Co−Cu, −0.8 V, 15 min	M_1	P	DL
	t_m [s]	177	900	
	J_m [10^{-3} A cm^{-2}]	1.353	0.28	
$J_{3DI\text{-}Li}$	k_2 [10^{-9} mol cm^{-2} s^{-1}]		5.90	
	$N_0k_1^2$ [10^{-9} mol^2 cm^{-6} s^{-2}]		5.99	
$J_{3DP\text{-}DC}$	K	0.13		
	D_0 [10^{-6} cm^2 s^{-1}]	5.33		
	N_0 [10^3 cm^{-2}]	3.37		
J_{ads}	Q_{ads} [mC cm^{-2}]			19.85
	k_{ads} [mA cm^{-2}]			1.63
	k_{des} [s^{-1}]			0.082

electrodes, from sulfate solutions. These authors find at pH 3 a single stage where the mechanism is purely 3DP-Vd.

Co_xCu_{100-x}/Cu Bilayer. Films $Co_{63}Cu_{37}$ (−08 V/12 min)/brass acted as new substrates onto which the second layer (copper) is deposited at −0.8 V during 15 min. A typical CTT curve is shown in Figure 7a, with a maximum M_1 corresponding to a 2DP nucleation regime for $t/t_m < 1$ and 2DI for $t/t_m > 1$, and maxima M_2, M_3, and M_4 following the theoretical 3DP curve (see Figure 7b). The contribution J_{ads} is that previously defined. The total current density is then:

$$J(t) = J_{ads\text{-}DL}(t) + J_{2DI\text{-}Li/2DP\text{-}Li}(t) + J_{3DP\text{-}Li}(t) + J_{3DP\text{-}Li}(t) + J_{3DP\text{-}Li}(t) \quad (13)$$

It is known[6,10] that the transient for nucleation and three-dimensional growth can be derived directly from those for two-dimensional growth. Also, the most important models assume either that each 3D nucleus forms on top of a single 2D growth center, after an induction period and at the same 2D and 3D nucleation rate, or that there is a competitive nucleation of 2D and 3D nuclei. In the two initial stages of our transients, represented by curves M_1 and M_2 (Figures 6a and 7a), a 3DP nucleation process on top of the 2D layer is likely to take place. In this sense, the kinetic parameter $AN_0k_g^2$ reaches values corresponding to the 2D instantaneous/progressive nucleation, which are larger than those ($AN_0k_1^2$) corresponding to the progressive 3D nucleation, that further decrease with the deposition time (see Table 7).

In late stages of Cu electrocrystallization, a 3DP-Li mechanism predominates. This gives place to a particular morphology in the samples (see micrographs in Figure 11), which is consistent with the growth of right-circular cones on the surface, that stopped growing at certain time (Scheme 1). A similar morphology was found when Cu was deposited onto brass and Co/brass substrate. Current−time transients show maxima (curves M_2, M_3, M_4 in Figures 6a and 7b), because the progressive stopping of all growth sites inevitably causes the current to approach zero with increasing time.

Table 5. S−H,[14] AFT,[17] and BFT[15] Theory Parameters for $Co_{63}Cu_{37}$/Brass, 30 min, and Kinetic Parameters of Langmuir Adsorption for the Electrochemical Double Layer (DL) Charge[18]

	Co−Cu, −0.8 V, 30 min	M_1	M_2	P	DL
	t_m [s]	200	1221	1800	
	J_m [10^{-3} A cm^{-2}]	1.102	0.261	0.20	
$J_{2DI\text{-}Li}$	h [10^{-6} cm]		1.83		
	$N_0k_g^2$ [10^{-9} mol^2 cm^{-6} s^{-2}]		2.36		
$J_{3DI\text{-}Li}$	$10^{-10}k_2$ [mol cm^{-2} s^{-1}]		5.40		
	$10^{-9}N_0k_1^2$ [mol^2 cm^{-6} s^{-2}]		3.27		
$J_{3DI\text{-}Vd}$	K	0.13			
	D_0 [10^{-6} cm^2 s^{-1}]	4.00			
	N_0 [10^3 cm^{-2}]	3.85			
$J_{3DP\text{-}Li}$	$AN_0k_1^2$ [10^{-12} mol^2 cm^{-6} s^{-3}]			2.51	
	k_2 [10^{-10} mol cm^{-2} s^{-1}]			4.15	
$J_{ads\text{-}DL}$	Q_{ads} [mC cm^{-2}]				17.1
	k_{ads} [mA cm^{-2}]				1.5
	k_{des} [s^{-1}]				0.087

DOI: 10.1021/acs.jpcc.6b04994
J. Phys. Chem. C 2016, 120, 22142−22154

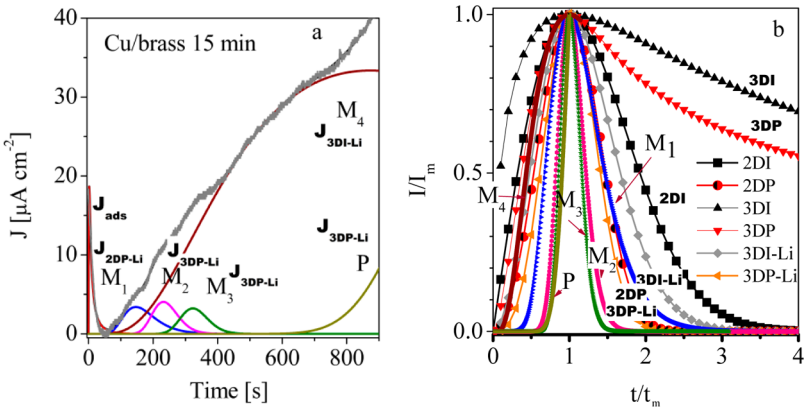

Figure 6. (a) CTT Cu/brass at −0.8 V for 15 min. (b) Dimensionless curves J/J_m vs t/t_m corresponding to CTT Cu/brass.

Table 6. BFT and AFT Theory Parameters for Cu/Brass in Progressive Process[15,17]

	Cu, −0.8 V, 15 min	M$_1$	M$_2$	M$_3$	M$_4$	P
	t_m [s]	147	232	323	874	900
	J_m [10^{-4} A cm^{-2}]	1.26	1.49	1.214	11.94	2.94
J_{2DP-Li}	h [10^{-7} cm]	3.41				
	$AN_0k_g^2$ [10^{-7} mol^2 cm^{-6} s^{-2}]	5.86				
J_{3DI-Li}	k_2 [10^{-9} mol cm^{-2} s^{-1}]				9.89	
	$N_0k_1^2$ [10^{-9} mol^2 cm^{-6} s^{-2}]				5.74	
J_{3DP-Li}	$AN_0k_1^2$ [10^{-10} mol^2 cm^{-6} s^{-3}]		10.5	3.90		0.18
	k_2 [10^{-9} mol cm^{-2} s^{-1}]		3.09	2.52		6.1
J_{ads-DL}	Q_{ads} [mC cm^{-2}]	7				
	k_{ads} [mA cm^{-2}]	0.5				
	k_{des} [s^{-1}]	0.075				

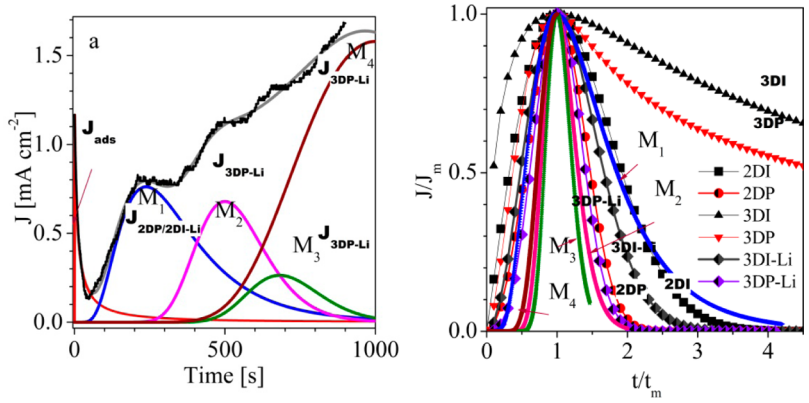

Figure 7. (a) CTT of Cu (−0.8 V/15 min), deposited onto $Co_{63}Cu_{37}$ (−0.8 V/12 min)/brass. (b) Dimensionless J/J_m vs t/t_m curves.

Table 7. BFT and AFT Theory Parameters for Cu Deposited onto $Co_{63}Cu_{37}$/Brass

	$Co_{63}Cu_{37}$/Cu, −0.8 V, 15 min	M$_1$	M$_2$	M$_3$	M$_4$
	t_m [s]	238	500	682	998
	J_m [10^{-4} A cm^{-2}]	7.687	6.85	2.70	15.86
J_{2DI-Li}	h [10^{-6} cm]	11			
	$N_0k_g^2$ [10^{-8} mol^2 cm^{-6} s^{-2}]	5.58			
J_{2DP-Li}	h [10^{-6} cm]	6.55			
	$AN_0k_g^2$ [10^{-10} mol^2 cm^{-6} s^{-2}]	9.38			
J_{3DP-Li}	$AN_0k_1^2$ [10^{-11} mol^2 cm^{-6} s^{-3}]		10.5	4.15	1.32
	k_2 [10^{-8} mol cm^{-2} s^{-1}]		1.42	0.56	3.28
J_{ads-DL}	Q_{ads} [mC cm^{-2}]	10.41			
	k_{ads} [mA cm^{-2}]	0.60			
	k_{des} [s^{-1}]	0.058			

DOI: 10.1021/acs.jpcc.6b04994
J. Phys. Chem. C 2016, 120, 22142−22154

Scheme 1. Schematic Side View of a Film Illustrating a 3DP Nucleation Process on Top of the 2D Layer

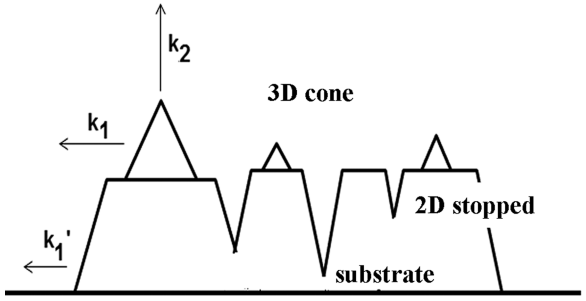

3.2. Film Properties. *Microstructures.* The X-ray diffractogram for 2θ between 30° and 95° of the polished $Cu_{70}Zn_{30}$ substrate is shown in Figure 8. The main peaks are identified as

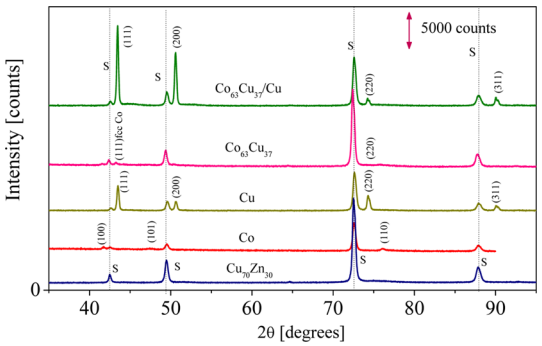

Figure 8. XRD patterns of Co, Cu, and Co−Cu films electrodeposited onto brass; that corresponding to the $Cu_{70}Zn_{30}$ substrate is provided for comparison. The vertical line in the upper right corner provides the ordinate scale.

fcc brass lines, and their relative heights indicate a large (111) texture, as expected for these heavily laminated substrates. X-ray diffraction of Cu films electrodeposited at −0.8 V/15 min indicates they are *fcc* and polycrystalline, with a good correspondence with electrolytic copper prepared by AC (JCPDS 00-003-1018).[25] The maximum intensity at 2θ = 43,45° corresponds to the (111) main Cu line; lines corresponding to (200), (220), and (311) planes are observed at 50.57°, 74.20°, and 89.90°, respectively. A mean crystallite size of 37 ± 5 nm and a cell parameter a_0 = 3.604(2) Å are estimated. Co films, prepared at −0.8 V by 30 min, are *hcp* (JCPDS 00-005-0727).[26] Lines clearly different from those of the substrate are observed at 2θ of 41.68°, 44.72°, 47.40°, and 76.08°, corresponding to (100), (002), (101), and (110) planes, with a (100) texture. The grain size estimated using the Scherrer equation was 28 ± 6 nm, and the hexagonal cell parameters were a = 2.507(3) Å and c = 4.09(3) Å. X-ray diffractogram corresponding to $Co_{63}Cu_{37}$ films after 30 min deposition is also depicted in Figure 8. It is known that the compact hexagonal structure is preferential for pure cobalt deposition; however, in the presence of copper and with potentiostatic electrodeposition methods, cobalt tends to stabilize in the cubic structure.[25] Next, (111) (220) *fcc* Co lines [JCPDS 00-015-0806][25,26] may be observed. The estimation of grain size from the (111) peak using the Scherrer equation was 38 ± 8 nm, and the cubic cell parameter is a = 3.62(4) Å. When Cu is deposited onto $Co_{63}Cu_{37}$/brass films, the Cu *fcc* (111) peak locates near that of the Co(Cu) solid solution; in this case, no estimation of crystallite size from the peak width is performed.

After 30 min of deposition, Co layers (Figure 9a) have $h \approx 1$ μm thick and exhibit a textured, irregular surface, probably due

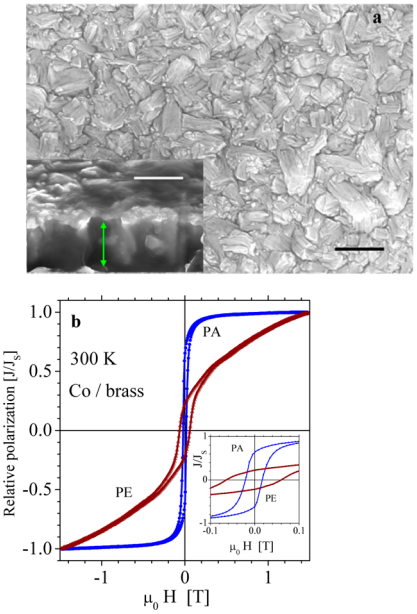

Figure 9. (a) SEM image of a Co deposit (bar = 1 μm); a side view of the film is shown in the inset (bar = 1 μm) where the film height is indicated by an arrow. (b) Room-temperature hysteresis loops corresponding to an as-deposited Co film, measured in both configurations, with the applied magnetic field parallel (PA) and perpendicular (PE) to the layer plane.

to side reactions such as H_2 evolution during the electrodeposition. It has been reported that adsorbed H stabilizes the [110] orientation while H_2 favors the [210] orientation.[4]

The electrocrystallization mechanisms of alloyed Fe−Co thick films on Cu substrates have been recently reported;[22] depending on the iron alloy content, different kinetics and microstructures are observed. Co deposition on Cu substrates is well described by a 3DP-Vd mechanism. Regarding the microstructure, dense, large agglomerates (100−300 nm) of quite equiaxed particles (average 50 nm) form, with mean crystallite sizes of 23 nm for *hcp* Co and 29 nm for *fcc* Co. In Co films on brass, studied in the present work, an initial 3DI nucleation regime is observed, with a transition to a 3DP-Vd one; then, in later stages, 3DP-Li mechanisms predominate. On brass, only *hcp* Co deposits and structures are coarser, with many columnar grains 500 nm to 1 μm diameter and a mean crystallite size of about 28 nm.

$Co_{63}Cu_{37}$ alloys obtained from a single electrolyte are inspected by SEM. Figure 10a shows an upper view of the film obtained after 15 min deposition, in which a regular particulate-like morphology is evident. "Particles" have 150 nm of apparent diameter and show definite facets. The first stage of the process is found to follow a 3DI regime, with an instantaneous nucleation mode; the deposited crystallite morphology is uniform in size and shape (prismatic), which is consistent with a multidirectional three-dimensional growth pattern. A similar morphology has been reported for short times in Co−Cu films deposited onto glassy carbon,[24] indicating an instantaneous nucleation process as that considered in the Scharifker and Hill model.[14] In the long

DOI: 10.1021/acs.jpcc.6b04994
J. Phys. Chem. C 2016, 120, 22142−22154

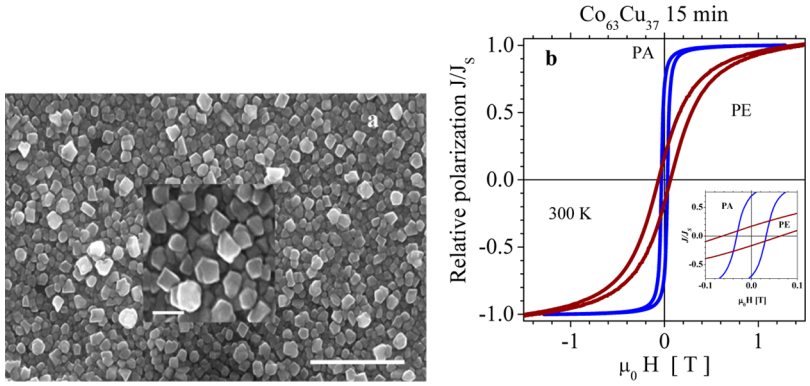

Figure 10. (a) SEM image of $Co_{63}Cu_{37}$ film (bar = 1 μm). Details are illustrated in the central inset (bar = 150 nm). (b) Room-temperature hysteresis loops corresponding to the film in (a), measured in both configurations, with the applied magnetic field parallel (PA).

term (t > 500 s), a mechanism involving 3D progressive regime initiates, which is controlled by incorporation at the interface.

$Co_{63}Cu_{37}$/Cu bilayer surface is shown in Figure 11a; the inset provides a lateral view of the bilayer, where the initial layer

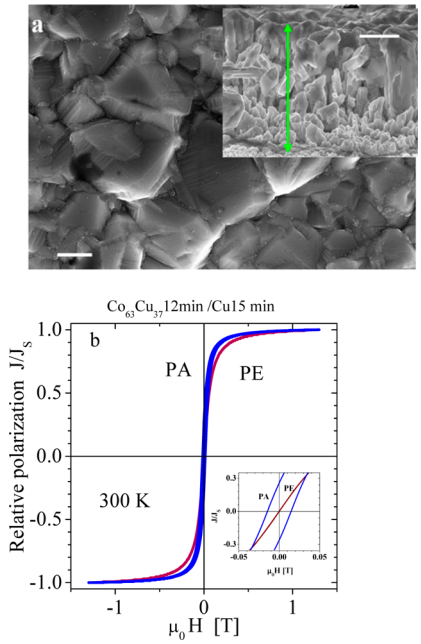

Figure 11. (a) SEM image (bar = 1 μm) of Cu deposited onto $Co_{63}Cu_{37}$/brass (12′); a side view of the film is shown in the inset (bar = 1 μm) where the film height is indicated by an arrow. (b) Room-temperature hysteresis loops corresponding to as-deposited Cu film onto $Co_{63}Cu_{37}$/brass (12′) substrate, measured in both configurations, with the applied magnetic field parallel (PA) and perpendicular (PE) to the layer plane.

of particulate morphology (as that shown in Figure 10a) and the second Cu layer of about 3 μm thickness are shown.

Magnetic Hysteresis. Room-temperature hysteresis loops corresponding to the as-deposited film were measured in both configurations, with the applied magnetic field parallel (PA) and perpendicular (PE) to the layer plane. The total magnetic moment of the assembly has a contribution from the diamagnetic brass support, so the ferromagnetic component must be estimated after subtracting a linear contribution with negative susceptibility.

Films are soft ferromagnetic, and they all exhibit an in-plane easy magnetization axis; however, a larger coercivity is measured for fields applied perpendicular to the film plane in single layer Co and $Co_{63}Cu_{37}$ films. The $Co_{63}Cu_{37}$/Cu bilayer exhibits little shape anisotropy as long as the loops are similar for the two normal directions, PA and PE, of the applied field.

The hysteresis loops in Figures 9 and 10 actually show a larger coercivity along the perpendicular direction than in the in-plane direction, particularly in *hcp* Co films. This suggests that other contributions to the magnetic anisotropy, in addition to shape anisotropy and with an out-of-plane easy axis, may exist.

It is not clear at present if this phenomenon is due to texture effects (Co film exhibits (100) hexagonal texture and $Co_{63}Cu_{37}$ films a cubic (111) one) or to internal stresses developed during deposition. In this sense, no large strains were detected by XRD techniques.

The high value of the saturation magnetization and low coercivity of these films both match the requirements for technological applications.

Hysteresis loops are similar to those obtained for Fe−Co films[22] deposited on Cu foil in the sense that they present an in-plane easy axis and an out-of-plane hard axis; also, all of the samples exhibit a coercive field slightly larger when the magnetic field is applied perpendicular (PE) to the film plane, indicating that the easy is also the soft axis.

4. CONCLUSIONS

The electrocrystallization processes of Co, Cu, and Co_xCu_{100-x} alloy thick films, and of double layer Co_xCu_{100-x}/Cu thick films, onto a Cu-30 wt % Zn brass substrate are characterized. The nucleation and growth kinetics are described for relatively long deposition times on the basis of single ion theoretical models, even in the case of binary alloys. The results indicate that successive nucleation and growth steps take place during the process. When the $J-t$ transient profile shows several maxima, they may be identified and analyzed as separate processes. In pure Co and Co-rich samples, the first maximum undergoes instantaneous nucleation with a 3D diffusion-controlled growth; subsequent maxima exhibit a progressive character. Cu deposited onto brass and onto $Co_{63}Cu_{37}$ alloy films undergoes a mechanism of progressive nucleation at all steps, changing from 2D nuclei in the first step to a 3D geometry in the later ones. Morphologies and grain textures observed by SEM confirm the preferred columnar growth in Co, and a prevalecence of 3D growth in Cu deposits. Co-containing films

DOI: 10.1021/acs.jpcc.6b04994
J. Phys. Chem. C 2016, 120, 22142−22154

are soft ferromagnetic, with in-plane easy magnetization axis arising from magnetostatic shape effects. Co and Co-rich films exhibit crystallographic texture leading to a larger coercivity when the magnetic field is applied normal to the film plane.

APPENDIX

Given the complexity of the observed transients in the present case of Cu−Co depositions, different regimes have to be considered, and the corresponding dimensionless j/j_m versus t/t_m curves constructed.

Scharifker−Hills Models[14]

The 3DI-Vd current transient is described in the Scharifker−Hills model by the expression:

$$J_{3DI\text{-}Vd}(t) = \frac{zFD_0^{1/2}c}{\pi^{1/2}t^{1/2}}\{1 - \exp[-N_0\pi kD_0t]\} \tag{A1}$$

with

$$k = \left[\frac{8\pi cM}{\rho}\right]^{1/2}$$

zF [C mol^{-1}] is the molar charge transferred during the electrodeposition/dissolution process, F = 96 500 C mol^{-1} is the Faraday constant, N_0 is the density number of isolated centers, $c = 1 \times 10^{-4}$ mol cm^{-3} is the molar concentration, and ρ and M are the metal density and molecular weight, respectively. D_0 is the effective diffusion coefficient. Differentiating eq A1 and equating the expression to zero, t_m and j_m values corresponding to the current maximum can be determined, leading to the effective diffusion coefficient:

$$D_o = \frac{j_m^2 t_m}{0.1629[zFc]^2} \tag{A2}$$

and to a nucleation rate or nuclear density number N_0:

$$N_0 = \left[\frac{1.2564}{\pi kD_0t_m}\right] \tag{A3}$$

In the case of a progressive regime,[14] the current is described by the equation:

$$J_{3DP\text{-}Vd}(t) = \frac{zFD_0^{1/2}c}{\pi^{1/2}t^{1/2}}\left\{1 - \exp\left[-\frac{AN_\infty\pi k'D_0t^2}{2}\right]\right\} \tag{A4}$$

with

$$k' = \frac{4}{3}\left[\frac{8\pi cM}{\rho}\right]^{1/2} \tag{A5}$$

The diffusion coefficient and the nucleation speed then may be estimated as

$$D_0 = \frac{i_m^2 t_m}{0.2598[zFc]^2} \tag{A6}$$

$$AN_\infty = \left[\frac{4.6733}{\pi k'D_0t_m^2}\right] \tag{A7}$$

with

$$N_s = \left[\frac{J}{2k'D_0}\right]^{1/2} \tag{A8}$$

Here A [s^{-1}] is the nucleation rate constant, $J = AN_\alpha$ is the nucleation speed, and N_s is the saturation nuclear sites density.

Bewick, Fleischmann, and Thirsk Model[15]

For 2D-Li processes limited by incorporation (separation) of atoms to (from) the nucleus, the transient currents are given by

$$J_{2DI\text{-}Li}(t) = \frac{2\pi zFMhN_0k_g^2}{\rho}t\exp\left(-\frac{\pi M^2N_0k_g^2}{\rho^2}t^2\right) \tag{A9}$$

and

$$J_{2DP\text{-}Li}(t) = \frac{\pi FMhAN_0k_g^2}{\rho}t^2\exp\left(-\frac{\pi M^2AN_0k_g^2}{3\rho^2}t^3\right) \tag{A10}$$

where zF [C mol^{-1}] is the molar charge, k_g is the nucleus lateral growth-rate constant [mol cm^{-2} s^{-1}], h [cm] is the layer thickness, N_0 is the number density of isolated centers, M [g mol^{-1}] is the molecular weight, and ρ [g cm^{-3}]is the density of the deposited material. As before, the current density J_m and the time t_m, corresponding to the point of the maximum current density, can be evaluated by equating the first derivative to zero. From eq A9 were derived eqs A11, A12, and A13, and the parameters $k_g^2N_0$ and the layer thickness h may be determined.

$$t_m = \left(-\frac{\rho^2}{2\pi M^2N_0k_g^2}\right)^{1/2} \tag{A11}$$

$$J_m = \frac{(2\pi)^{1/2}zFhN_0^{1/2}k_g}{\rho}\exp\left(-\frac{1}{2}\right) \tag{A12}$$

$$J_mt_m = \frac{(zF\rho h)}{M}\exp\left(-\frac{1}{2}\right) \tag{A13}$$

In the same way, parameters $Ak_g^2N_0$ and h [cm] for the progressive regime may be estimated from eqs A10, A14, A15, and A16.

$$t_m = \left(-\frac{2\rho^2}{\pi M^2AN_0k_g^2}\right)^{1/3} \tag{A14}$$

$$J_m = zF\left(\frac{4\pi AN_0k_g^2\rho}{M}\right)^{1/3}h\exp\left(-\frac{2}{3}\right) \tag{A15}$$

$$J_mt_m = \frac{(2zF\rho h)}{M}\exp\left(-\frac{2}{3}\right) \tag{A16}$$

Armstrong−Fleischmann and Thirsk[17]

The current density $j(t)$ for a 3DI-Li process may be described by the expression:

$$J(t)_{3DI\text{-}Li} = zFk_2\left\{1 - \exp\left[-\frac{\pi M^2k_1N_ot^2}{\rho^2}\right]\right\} \times \exp\left(-\frac{\pi M^2N_0k_1^2t^2}{\rho^2}\right) \tag{A17}$$

where z, F, M, N_0, and ρ have the above indicated meaning; k_1 is the nucleus lateral growth-rate constant [mol cm^{-2} s^{-1}], and k_2 is the nucleus vertical growth-rate constant [mol cm^{-2} s^{-1}]. The current density J_m and the time t_m, corresponding to the

DOI: 10.1021/acs.jpcc.6b04994
J. Phys. Chem. C 2016, 120, 22142−22154

point of the maximum current density, were evaluated by equating the first derivative of the relation $J-t$ to zero, then:

$$t_m = \left[\frac{\rho^2}{\pi M^2 N_0 k_1^2} \ln 2\right]^{1/2} \quad (A18)$$

$$j_m = \left[\frac{zFk_2}{4}\right] \quad (A19)$$

and

$$j_m t_m = 0.25 zFk_2 \left[\frac{\rho^2 \ln 2}{\pi M^2 N_0 k_1^2}\right]^{1/2} \quad (A20)$$

The current density in a 3DP process is given by

$$J(t)_{3DP\text{-}Li} = zFk_2\left\{1 - \exp\left[-\frac{\pi M^2 k_1 A N_0 t^3}{3\rho^2}\right]\right\} \times \exp\left(-\frac{\pi M^2 N_0 A k_1^2 t^3}{3\rho^2}\right) \quad (A21)$$

with the resulting parameters:

$$t_m = \left[\frac{3\rho^2}{\pi M^2 N_0 A k_1^2} \ln 2\right]^{1/3} \quad (A22)$$

$$j_m = \left[\frac{zFk_2}{4}\right] \quad (A23)$$

and

$$j_m t_m = 0.25 zFk_2 \left[\frac{3\rho^2 \ln 2}{\pi M^2 A N_0 k_1^2}\right]^{1/3} \quad (A24)$$

Here, A $[s^{-1}]$ is the nucleation rate constant, k_1 is the nucleus lateral growth-rate constant [mol cm^{-2} s^{-1}], k_2 is the nucleus vertical growth-rate constant, and the other parameters have the previously defined meaning.

The dimensionless curves corresponding to eqs A1, A4, A9,A10, A17, and A21 are given as eqs 1−6, respectively, in the main text.

■ ASSOCIATED CONTENT

Supporting Information

The Supporting Information is available free of charge on the ACS Publications website at DOI: 10.1021/acs.jpcc.6b04994.

Contribution of the less noble substrate components to the current response during deposition, and boron content in the films (PDF)

■ AUTHOR INFORMATION

Corresponding Author

*Tel.: +54-351-433 4051, ext 125. Fax: +54-351-433 4054. E-mail: carmenaguirre@famaf.unc.edu.ar.

Notes

The authors declare no competing financial interest.

■ ACKNOWLEDGMENTS

We thank FONCYT-PICT 0074-Argentine, and Secyt-UNC-Argentine, Program 2014-2015, Cod. P 05/BP13, for financial support.

■ REFERENCES

(1) Bland, J. A. C., Heinrich, B., Eds. *Ultrathin Magnetic Structures I and II*; Springer: Berlin-Heidelberg, 1994.

(2) Milchev, A. *Electrocrystallization. Fundamentals of Nucleation and Growth*; Kluwer Academic Publishers: New York, Boston, Dordrecht, London, Moscow, 2002.

(3) Uhlemann, M.; Gebert, A.; Herrich, M.; Krause, A.; Cziraki, A.; Schultz, L. Electrochemical Deposition and Modification of Cu/Co-Cu Multilayer. *Electrochim. Acta* **2003**, *48*, 3005−3011.

(4) Budevski, E.; Staikov, G.; Lorenz, W. J. In *Electrochemical Phase Formation and Growth*; Bar, M., Ed.; VCH Verlagsgesellschaft mbH: Weinheim, 1996; p 282.

(5) Gu, M.; Yang, F. Z.; Huang, L.; Yao, Z. B.; Zhou, S. M. Identification of Different Cobalt Nucleation on Glassy Carbon. *Chin. Chem. Lett.* **2004**, *15*, 981.

(6) Abyaneh, M. Y.; Vissche, W.; Barendrecht, E. Study of the Electrocrystallization of Nickel by Ellipsometry. *Electrochim. Acta* **1983**, *28*, 285−291.

(7) Grujicic, D.; Pesic, B. Electrodeposition of Copper: The Nucleation Mechanisms. *Electrochim. Acta* **2002**, *47*, 2901.

(8) Ríos-Reyes, C. H.; Granados-Neri, M.; Mendoza-Huizar, L. H. Kinetic study of the cobalt electrodeposition onto glassy carbon electrode from ammonium sulfate solutions. *Quim. Nova* **2009**, *32* (No. 9), 2382−2386.

(9) Bijani, S.; Schrebler, R.; Dalchiele, E. A.; Gabás, M.; Martínez, L.; Ramos-Barrado, J. R. Study of the Nucleation and Growth Mechanisms in the Electrodeposition of Micro-and Nanostructured Cu_2O Thin Films. *J. Phys. Chem. C* **2011**, *115*, 21373.

(10) Abayaneh, M. Y.; Fleischmann, M. The Electrocrystallisation of Nickel Part I. Generalized Models of Electrocrystallisation. *J. Electroanal. Chem. Interfacial Electrochem.* **1981**, *119*, 187.

(11) Mendoza-Huizar, L. H.; Ríos-Reyes, C. H. Underpotential Deposition of Cobalt onto Polycrystalline Platinum. *J. Solid State Electrochem.* **2011**, *15*, 737.

(12) Palomar-Pardavé, M.; Miranda-Hernández, M.; González, I.; Batina, N. Detailed Characterization of Potentiostatic Current Transients with 2D-2D and 2D-3D Nucleation Transitions. *Surf. Sci.* **1998**, *399*, 80−95.

(13) Mendoza-Huizar, L. H.; Robles, J.; Palomar-Pardavé, M. Nucleation and Growth of Cobalt onto Different Substrates Part I. Underpotential Deposition onto a Gold Electrode. *J. Electroanal. Chem.* **2002**, *521*, 95−106.

(14) Sharifker, B.; Hill, G. Theoretical and Experimental Studies of Multiple Nucleation. *Electrochim. Acta* **1983**, *28*, 879−889.

(15) Bewick, A.; Fleischmann, M.; Thirsk, H. R. Kinetics of the Electrocrystallization of thin films of calomel. *Trans. Faraday Soc.* **1962**, *58*, 2200−2216.

(16) Martinez-Ruíz, A.; Palomar-Pardavé, M.; Batina, N. Over-potential Deposition of Copper on an Iodine-modified Au(111) Electrode. *Electrochim. Acta* **2008**, *53*, 2115−2120.

(17) Armstrong, R. D.; Fleischmann, M.; Thirsk, H. R. The Anodic Bbehavior of Mercury in Hydroxide Ion Solutions. *J. Electroanal. Chem.* **1966**, *11*, 208−223.

(18) Hölzle, H.; Retter, U.; Kolb, D. M. The Kinetics of Structural Changes in Cu Adlayers on Au(111). *J. Electroanal. Chem.* **1994**, *371*, 101−109.

(19) Milchev, A.; Zapryanova, T. Nucleation and Growth of Copper Under combined Charge Transfer and Diffusion Limitations. *Electrochim. Acta* **2006**, *51*, 2926−2933.

(20) Cotton, A.; Wilkinson, G. *Advanced Inorganic Chemistry*, 3rd ed.; Wiley: New York, 1972.

(21) Santos, J. S.; Matos, R.; Trivinho-Strixino, F.; Pereira, E. C. Effect of Temperature on Co Electrodeposition in the Presence of Boric Acid. *Electrochim. Acta* **2007**, *53*, 644−649.

(22) Aguirre, M. del C.; Farías, E.; Abraham, J.; Urreta, S. E. $Co_{100-x}Fe_x$ Magnetic Thick Films Prepared by Electrodeposition. *J. Alloys Compd.* **2015**, *627*, 393−401.

DOI: 10.1021/acs.jpcc.6b04994
J. Phys. Chem. C 2016, 120, 22142−22154

(23) Yu, Y.; Song, Z.; Ge, H.; Wei, G.; Jiang, L. Electrochemical Mechanism of Cobalt Film Electrodeposition Process. *Mater. Res. Innovations* **2016**, *20*, 280−284.
(24) Gu, M. Initial Stages of the Electrocrystallization of Co-Cu Alloys on GCE from the Co Rich Electrolytes. *Electrochim. Acta* **2007**, *52*, 4443−4448.
(25) Joint Committee on Powder Diffraction Standards, Diffraction Data File, no. 34-1354 JCPDS International Center for Diffraction Data, Pennsylvania, 1991.
(26) Joint Committee on Powder Diffraction Standards, Diffraction Data File, no. 05-0727 JCPDS International Center for Diffraction Data, Pennsylvania, 1991.

DOI: 10.1021/acs.jpcc.6b04994
J. Phys. Chem. C 2016, 120, 22142−22154